

Dynamical spin susceptibility in La_2CuO_4 studied by resonant inelastic x-ray scattering

H. C. Robarts,^{1,2} M. García-Fernández,¹ J. Li,^{1,3} A. Nag,¹ A. C. Walters,¹ N. E. Headings,² S. M. Hayden,^{2,*} and Ke-Jin Zhou^{1,†}

¹*Diamond Light Source, Harwell Campus, Didcot OX11 0DE, United Kingdom*

²*H. H. Wills Physics Laboratory, University of Bristol, Bristol BS8 1TL, United Kingdom*

³*Beijing National Laboratory for Condensed Matter Physics and Institute of Physics, Chinese Academy of Sciences, Beijing 100190, China*

Resonant inelastic X-ray scattering (RIXS) is a powerful probe of elementary excitations in solids. It is now widely applied to study magnetic excitations. However, its complex cross-section means that RIXS has been more difficult to interpret than inelastic neutron scattering (INS). Here we report high-resolution RIXS measurements of magnetic excitations of La_2CuO_4 , the antiferromagnetic parent of one system of high-temperature superconductors. At high energies (~ 2 eV), the RIXS spectra show angular-dependent dd orbital excitations which are found to be in good agreement with single-site multiplet calculations. At lower energies ($\lesssim 0.3$ eV), we show that the wavevector-dependent RIXS intensities are proportional to the product of the single-ion spin-flip cross section and the dynamical susceptibility $\chi''(\mathbf{q}, \omega)$ of the spin-wave excitations. When the spin-flip cross-section is dividing out, the RIXS magnon intensities show a remarkable resemblance to INS data. Our results show that RIXS is a quantitative probe the dynamical spin susceptibility in cuprate and therefore should be used for quantitative investigation of other correlated electron materials.

I. INTRODUCTION

Unconventional superconductors constitute an important group of strongly-correlated electron materials that include heavy fermions, cuprates, ruthenates, and iron-based superconductors. [1–4]. They also show a proximity to magnetic ordering or have strong magnetic fluctuations [5]. In some cases, the superconductivity can be established by chemical doping or pressurizing a magnetic parent compound. Although the long-range magnetic order is suppressed by the external tuning, the short-range magnetic fluctuations are found to survive in the superconducting phase of many unconventional superconductors [6–12]. The importance of these magnetic fluctuations to the superconducting pairing mechanism has been a subject of many studies in the last decades [5, 13].

Experimentally, inelastic neutron scattering (INS) is a well-established probe for the magnetic fluctuations in magnetic materials providing direct measurement of the magnetic structure factor $S(\mathbf{Q}, \omega)$ [14]. For example, in La_2CuO_4 (LCO), the parent compound of the first reported cuprate superconductors, INS measurements have observed spin-wave excitations throughout the Brillouin zone [15, 16]. The excitations are described by large superexchange couplings within the CuO_2 planes which extend beyond nearest neighbours. INS has also shown that magnetic excitations persist over a large range wavevectors in superconducting cuprates [11]. They are particularly strong near the $(1/2, 1/2)$ position.

Compared to INS, RIXS is a newly emerged technique which has been proven to be a powerful tool for

probing magnetic excitations in transition metal oxides [17, 18]. Owing to its high cross-section and the micron-size focused X-ray beam, RIXS is advantageous over INS in measuring small samples and nanometer-thick films. By working at a resonance, RIXS is element specific thus particularly suited for probing magnetic fluctuations in complex systems with multiple magnetic elements. High-resolution RIXS measurements at the Cu L -edge in LCO showed spin excitations with similar dispersion as INS [19] and subsequent measurements on a range of doped cuprates have revealed new information about the damping and energy dependence of the spin fluctuations [12, 20–25]. INS measurements of collective magnetic excitations become technically challenging above about 500 meV because the background due to multiple scattering becomes large. RIXS does not suffer from this problem thus it has a major advantage for measuring high-energy excitations. However, the exact RIXS cross-section remains a challenge for fully quantitative interpretation of magnetic excitations. As such, relative comparison is often adopted for tracking intensities evolution as a function of temperature or the doping level [21, 22, 26]. In a previous study of doped $\text{La}_{2-x}\text{Sr}_x\text{CuO}_4$, a new procedure was used to determine the absolute wavevector-dependent susceptibility in which magnetic excitation intensities in LCO measured by RIXS were assumed to be equivalent to those obtained from INS [27].

Here we aim to improve the understanding of RIXS as a probe of magnetic excitations by characterising its cross-section. LCO is chosen because of extensive studies on its magnetic excitations made by INS. The RIXS measurements were performed on LCO single crystals with surface normals (001) and (100) which provide a good test for the geometrical dependent single ion cross-section of the orbital and the spin-flip excitations. The

* s.hayden@bristol.ac.uk

† kejin.zhou@diamond.ac.uk

sample with the surface normal (100) provides further access along the (h, h) direction in reciprocal space compared to previous RIXS measurements. We firstly compare the measured dd orbital excitations and the calculations using crystal-field theory (CFT) implemented in the many-body code QUANTY [28, 29]. Good agreement was obtained for both samples. The comparison was then extended to the magnetic excitations. The extracted wavevector-dependent susceptibilities $\chi'(\mathbf{Q})$ show a remarkable match with those seen by INS after dividing out the spin-flip excitations. We highlight that the established method can be readily applied to quantitative studies of magnetic excitations in other superconductors, such as ruthenates, nickelates, as well as general transition-metal oxides based magnetic materials.

II. RIXS EXPERIMENTS

The RIXS experiments were performed on single crystal samples of LCO which were grown using the travelling solvent floating zone technique. We describe LCO using its high-temperature tetragonal (HTT) I4/mmm crystal structure in which $a = b \simeq 3.8 \text{ \AA}$, $c \simeq 13.2 \text{ \AA}$. The momentum transfer \mathbf{Q} is defined in reciprocal lattice units (r.l.u.) as $\mathbf{Q} = ha^* + kb^* + lc^*$ where $\mathbf{a}^* = 2\pi/a$ etc. The energy of the scattered photons is given by $\hbar\omega = c|\mathbf{k}| - c|\mathbf{k}'|$ and momenta $\mathbf{Q} = \mathbf{k} - \mathbf{k}'$, where \mathbf{k} and \mathbf{k}' is the incident and scattered photon wavevector, respectively.

High-resolution RIXS spectra were acquired at the I21-RIXS Beamline at Diamond Light Source, United Kingdom. The incoming X-ray photon energy was tuned to the Cu L_3 resonance ($\simeq 931.5 \text{ eV}$) and we performed measurements with both linear horizontal (LH)/ π polarisation and linear vertical (LV)/ σ polarisation (Fig. 1). The total instrumental energy resolution has standard Gaussian distribution with the full width at the half-maximum of $\Delta E \simeq 37 \text{ meV}$. All RIXS measurements were conducted at 15 K.

Two different samples, LCO001 and LCO100, were prepared with the surface normals approximately (001) and (100) respectively. The samples were aligned and cleaved in-situ to expose a clean surface to the beam. Fig. 1 (a, b) shows how data were collected from LCO001 along $(h, 0)$ and (h, h) respectively. Fig. 1(c) shows how LCO100 was mounted on a 45° wedge such that $(1\bar{1}0)$ was perpendicular to the scattering plane. This allowed data to be collected along (h, h) to larger h . Because of the two-dimensionality of the magnetic excitations in cuprates, the in-plane wavevector (h, k) is varied by scanning the angle of incidence θ while keeping the scattering angle, Ω , fixed at 154° . The zero of θ ($\theta = 0$) is defined such that (110) is anti-parallel to \mathbf{k} and ‘‘grazing-in’’ \mathbf{k} probes negative h . Thus with LCO001, we access $(h, 0) = (-0.5, 0)$ to $(0.5, 0)$ and $(h, h) = (-0.35, -0.35)$ to $(0.35, 0.35)$. For LCO100, (h, h) is probed with a maximal in-plane wavevector of $(0.4, 0.4)$.

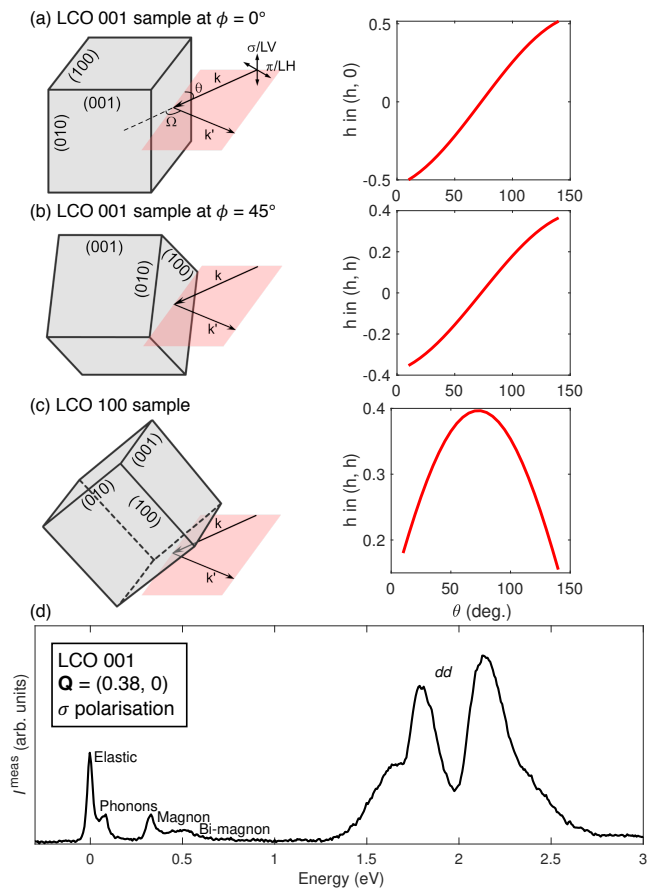


FIG. 1. RIXS experimental geometries for the two samples. (a) The LCO001 sample at $\phi = 0^\circ$, probing $(h, 0)$. (b) The LCO001 sample at $\phi = 45^\circ$, probing (h, h) . (c) The LCO100 sample probing (h, h) . For each orientation, the projection of the momentum transfer and the relationship between θ and the momentum transfer is shown. Panel (d) shows various excitations resolved in a typical RIXS spectrum.

A typical RIXS spectrum is shown in Fig. 1 (c) in which a quasi-elastic peak, phonon excitations, single-magnon, multimagnon, and dd orbital excitations are clearly resolved. The measured RIXS intensity, $I_{\sigma(\pi)}^{\text{meas}}$ can be corrected to yield the real RIXS intensity $I_{\sigma(\pi)}^{\text{corr}}$, to account for energy, wavevector and polarisation-dependent self-absorption effects. The self-absorption correction method is an extension of the simple procedure in recent works [30, 31] and is described explicitly in Appendix A 3. In Section III, we will firstly focus on the dd orbital excitations and in Section IV, we will discuss the magnetic excitations.

III. dd ORBITAL EXCITATIONS

The RIXS spectra are dominated by strong dd excitations between 1.3 and 3 eV which occur due to transitions between the ground and the excited $3d$ orbital states as sketched in Fig. 2 (a). dd excitations have been exten-

sively studied using RIXS in the past for understanding the local crystal field splittings among various cuprate families [32, 33]. Plotted in Fig. 2 (b) is a representative RIXS spectrum in the energy range of the dd excitations. A pseudo-Voigt function is used for the spectral fitting where each dd excitation seems to comprise two peaks. The higher energy peak in each orbital excitation is due to the mixture with the spin-flip. Such excitation has not been observed in previous experiments due to the limitation of the energy resolution [33]. There is also additional spectral weight present at a higher energy of 2.4 eV. This peak is seen in a previous work and has been attributed to oxygen vacancies which are thought to alter the crystal field acting on the Cu ions [33]. We fit this peak with an additional pseudo-Voigt function.

To reproduce the experimental observations, we used the single-site crystal-field multiplet theory (CFT) implemented in the many-body QUANTY code [28, 29] to calculate the dd excitations. To simulate the spin-flip excitation, an inter-atomic exchange integral of 100 meV is added along the (h, h) direction of the CuO_2 planes. Throughout the paper, all calculations were done with the outgoing polarisations effect averaged. Appendix B describes the calculation details. We assume that in the range of the dd excitations, the self-absorption corrected RIXS intensity can be described as a product of a pre-factor f' and the single-ion orbital cross-section $R_{\text{orbital}}(\epsilon, \epsilon', \mathbf{k}, \mathbf{k}')$:

$$I_{\text{orbital}} = f' \times R_{\text{orbital}}(\epsilon, \epsilon', \mathbf{k}, \mathbf{k}'). \quad (1)$$

Fig. 2 (b) compares the intensity of the orbital component, R_{orbital} , to the RIXS measurements for a representative spectra. The calculations seem to agree well with the experiments.

dd orbital excitations possess a strong angular dependence owing to the anisotropy of the Cu $3d$ orbitals [33]. In Fig. 2 (c-h) we summarize the integrated dd orbital excitation intensity as a function of θ under various experimental configurations. Note that each data point represents the sum of the integrated area of normal dd and the spin-flip assisted dd excitations.

Theoretically, θ -dependent dd excitations in LCO have been simulated successfully using the single-ion model [17, 33]. Here we use QUANTY to perform similar calculations. Fitted area of each calculated dd excitation is superimposed on the experiment data shown in Fig. 2 (c-h). Note that the calculated dd excitation intensities have been independently scaled to their respective orbitals. The overall comparison between the experiment and the theory yields a good consistency except some deviations at small grazing out angles. For instance, the d_{xz}/d_{yz} orbital in LCO001 with σ polarization and the d_{xy} orbital in LCO100 with both polarizations. This may be due to the accuracy of the fit at those extreme angles. The good agreement of the θ -dependent dd intensities suggest that the local dd cross-sections based on a single site multiplet theory reproduce the experimental data from samples with different crystal orientations very well.

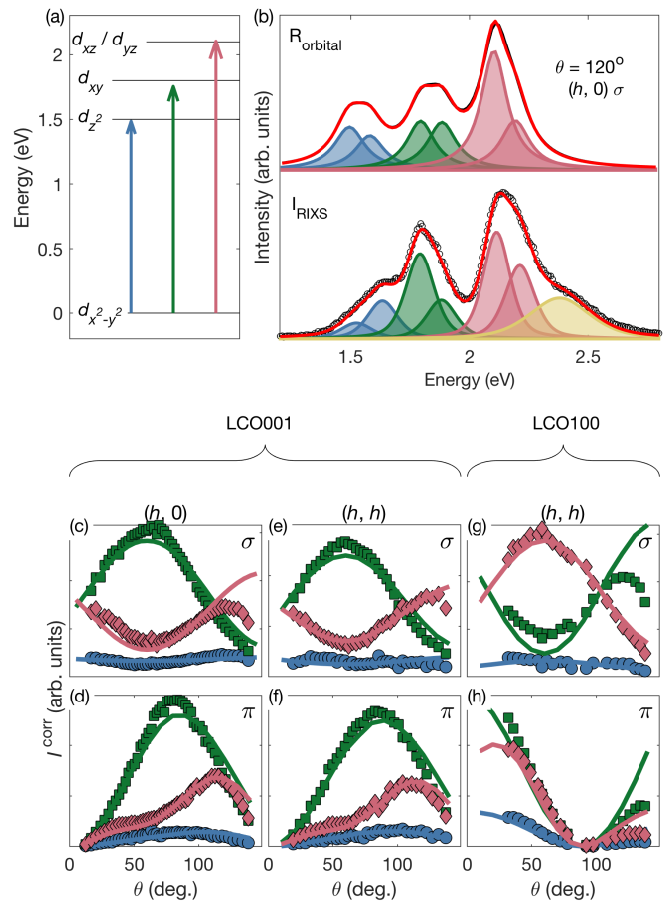


FIG. 2. Orbital excitations in RIXS showing (a) the dd transitions in LCO and (b) a comparison of the calculated dd peaks from crystal field theory (CFT) and RIXS measurements for a typical spectra at $\theta = 120^\circ$ along the $(h, 0)$ direction, LCO001 orientation and with σ polarisation. Panels (c-h) show the intensity of the dd excitations from fitted RIXS data compared with the relative intensities calculated in CFT.

We are therefore highly motivated to apply the theory to the magnetic excitations whose intensities are strongly θ dependent [17].

IV. DYNAMICAL SPIN SUSCEPTIBILITY

Fig. 3 (a-f) show RIXS intensity maps in the low energy region as a function of the momentum transfer along (100) and (110) directions. Near zero energy loss, we see quasi-elastic peaks. Between zero and 100 meV, two phonon branches are clearly resolved throughout the accessible momentum space. These are likely the bond-buckling and the bond-stretching modes [34] which will be discussed in a separate work. As is known, the strongly dispersive features are single magnons emanating from the zone center to the zone boundary up to almost 400 meV [15, 16]. In particular, single magnons in LCO100 show consistent dispersion compared to that

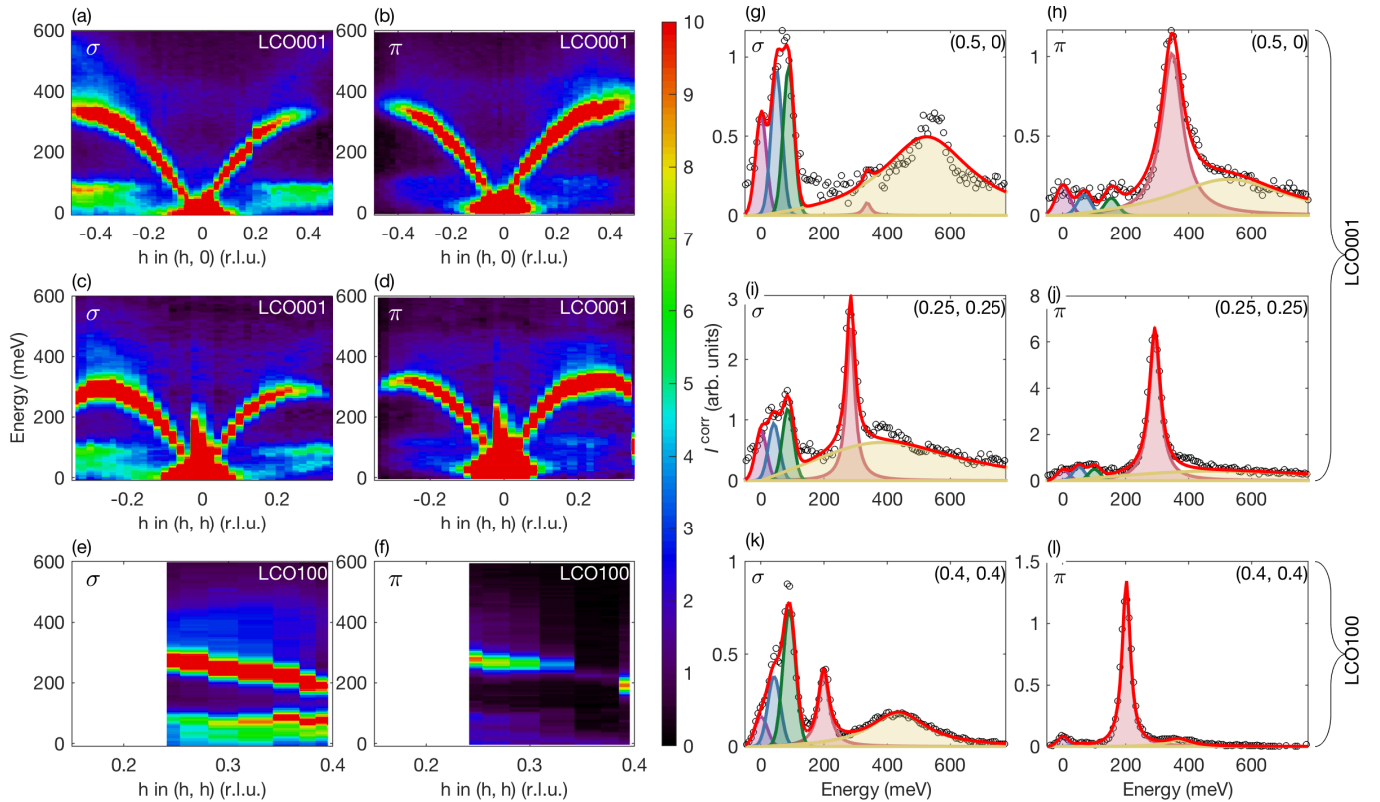


FIG. 3. The low-energy excitations in LCO showing (a-f) self-absorption corrected RIXS intensity maps and (g-l) representative RIXS spectra. Total fits to the data are shown in red. The DHO magnon and multimagnon fit are shown in pink and yellow respectively. Gaussian fits to the elastic peak, phonon and multiphonon peaks are in purple, blue and green respectively.

in LCO001 projected along the (h, h) direction. Beyond the zone boundary of $(1/4, 1/4)$, the single magnons continue to disperse to lower energy akin to the INS data (Fig.3(c)-(f)) [15, 16]. Broader peaks appear between 400 meV and 600 meV which are most likely the multimagnons as observed by RIXS at the Cu L_3 - and the O K - edges [35, 36].

The spectra between -80 and 800 meV are modelled with Gaussian functions to account for the elastic peak and phonons and with the response function of a damped harmonic oscillator (DHO) to account for the (single and multi) magnon excitations. The DHO model has been used in several RIXS studies [27, 37, 38] and describes the response for a range of damping. We fit the spectra to the imaginary part of the DHO response, given by,

$$\chi''(\mathbf{Q}, \omega) = \frac{\chi'(\mathbf{Q}) \omega_0^2(\mathbf{Q}) \gamma(\mathbf{Q}) \omega}{[\omega^2 - \omega_0^2(\mathbf{Q})]^2 + \omega^2 \gamma^2(\mathbf{Q})}, \quad (2)$$

where $\chi(\mathbf{Q})$ is the real part of the susceptibility at zero frequency, ω_0 describes the position of the excitation pole and γ represents the damping.

Examples of the RIXS spectra and fittings are shown in Fig. 3 (g-l). The data show drastically different ratio between the single and multimagnon intensity measured with incident polarisation σ or π . At $\mathbf{Q} = (1/2, 0)$, the single magnon component dominates the spectra for π

polarisation whilst it becomes much weaker and almost entirely obscured by the multimagnon component with σ polarisation. The drastic polarisation and θ dependence is due to the local spin-flip cross-section [17]. Strong multimagnon scattering is observed at the enigmatic region $(1/2, 0)$ under the σ polarisation where the profile are distinct to those in the rest of the reciprocal space.

To illustrate the single magnon dispersion more clearly, we plot the magnetic pole ω_0 of LCO001 in Fig. 4 (a-d). On top of that, we add data points obtained from LCO100 along the (h, h) direction. Noticeably, the single magnon dispersion obtained from LCO001 and LCO100 matches very well. To compare with the spin-wave theory (SWT), we computed the dispersion using the nearest and the next-nearest neighbour exchange constants extracted from INS [16]. Good agreement is seen in both $(h, 0)$ and (h, h) direction. Fig. 4 (e) and (f) shows comparisons of the magnon spectra obtained between RIXS and INS at two zone boundary positions. Remarkably, the lineshape of the magnon spectra agree well between two techniques. At the $(1/4, 1/4)$, the magnon excitation shows a resolution-limited peak whereas at $(1/2, 0)$, both RIXS and INS spectra present some spectral weight at high energy as a continuum.

We now discuss the RIXS intensity of the single magnons. As with the analysis of the dd excitations,

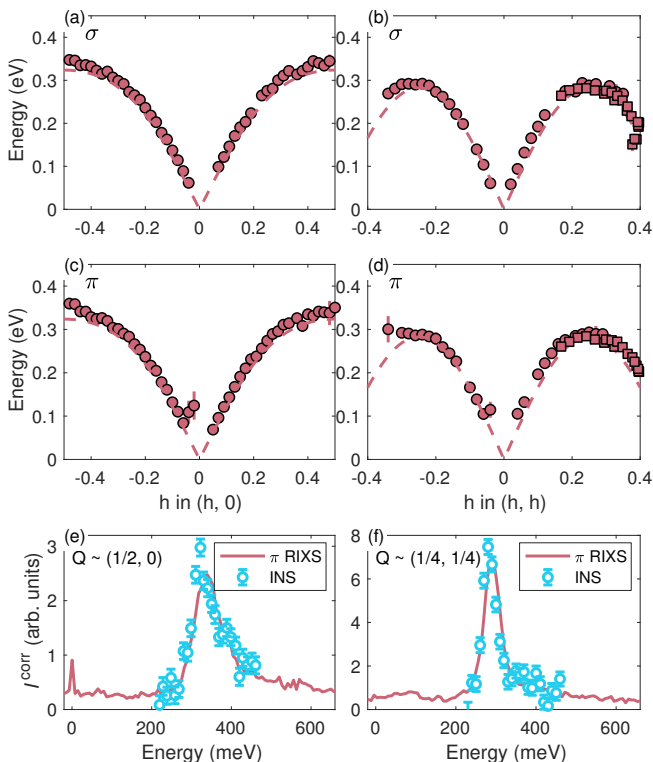


FIG. 4. (a-d) show the energy dispersion of magnon excitations measured by RIXS. Red symbols indicate ω_0 extracted from the damped harmonic oscillator fit to the magnons and data from the LCO001 and LCO100 orientations are indicated with circles and squares respectively. The dashed line shows the magnon dispersion extracted from INS [16]. Panels (e-f) show comparison of the magnon lineshape measured with π polarised RIXS in pink and INS in cyan, at wavevectors close to $(1/2, 0)$ and $(1/4, 1/4)$. The INS data are scaled to the RIXS data and a constant offset of 0.5 is added to the INS to compensate for a possible over subtraction of the background in Ref. [16].

the single magnon intensities are extracted from an integration of the DHO function and summarized in Fig. 5 (a-f). Note that these data are presented as a function of θ due to the complex projection along the (h, h) direction in LCO100. Importantly, as the single magnons are strongly dispersive in the energy-momentum space, an accurate self-absorption correction is performed for both the energy and momentum dependence. Details of the self-absorption correction are presented in Appendix A 3. It is generally accepted that under certain conditions [18], the RIXS intensity is proportional to the dynamic structure factor $S(\mathbf{Q}, \omega)$ multiplied by a resonant factor f which is dependent on the polarisation ϵ and ϵ' of the initial and final photons with wavevector \mathbf{k} and \mathbf{k}' . As the single-ion spin-flip cross-section is controlled by the RIXS process, we further express the resonant factor $f(\epsilon, \epsilon', \mathbf{k}, \mathbf{k}')$ as a product of a pre-factor f' and the

single-ion spin-flip cross-section $R_{\text{spin}}(\epsilon, \epsilon', \mathbf{k}, \mathbf{k}')$:

$$I_{\text{spin}} = f' \times R_{\text{spin}}(\epsilon, \epsilon', \mathbf{k}, \mathbf{k}') \times S(\mathbf{Q}, \omega). \quad (3)$$

Under this approximation, we computed the single-ion spin-flip cross-section, R_{spin} , as a function of θ using the parameters optimised for the dd calculations. The calculated spin-flip spectra were fitted using DHO function (Eqn. 2) and the integrated spectral weight are plotted on top of the experimental data in Fig. 5 (a-f).

The first glimpse informs us that the experimental magnon intensities modulate as a function of θ and follow the overall trend of the local spin-flip cross-section at least for LCO001. However there are deviations around $\theta \simeq 75^\circ$ where the magnon intensity drops almost to zero. This is probably due to the diminished spin wave intensity near the zone center. It is thus appealing to see both the local and the collective behaviors play a role in the magnon intensities in RIXS. For LCO100, it is less obvious to trace the evolution of the magnon intensities between the experiment data and the local spin-flip cross-section. This may be due to the unusual projection of the momentum transfer along the (h, h) direction.

To reveal the dynamic spin susceptibility from RIXS, we divided the magnon intensity by the local RIXS spin cross-section from the CFT calculations,

$$S(\mathbf{Q}, \omega)_{\text{RIXS}} \propto \frac{I_{\text{spin}}}{R_{\text{spin}}}. \quad (4)$$

$S(\mathbf{Q}, \omega)_{\text{RIXS}}$ is shown for both LCO001 and LCO100 in Fig. 5 (g-l) as a function of wavevector. Remarkably, the simple process yields a highly symmetrical intensity profile with respect to the zone center in LCO001 along both $(h, 0)$ and (h, h) directions. The symmetrical magnon intensity profile is reminiscent of the spin-wave intensity in the Heisenberg model [15, 16]. For LCO100, the difference after the removal of the local spin-flip cross-section is even more striking. The irregular magnon intensity profile evolved to a clear exponential-like trend as a function of \mathbf{Q} along the (h, h) direction. We want to bring the attention to the effect of the incident X-ray polarizations. The fact that there is almost no polarization dependence among all sets of data pointing to a simple message, that is, the pure collective dynamic spin susceptibility is independent of the property of the experimental probe. It is also worth mentioning the error bars of the magnon intensities. For LCO001, data points near the zone center are marked with large error bars due to the uncertainty of fitting the negligible raw magnon intensities. Similarly, the data points near the very grazing-out (grazing-in) geometry in $\sigma(\pi)$ polarization are associated with large error bars as a result of minimal local spin-flip cross-section. The latter reason also applies to LCO100 where the large error bars are present near $\theta \simeq 60^\circ$ and 90° for σ and π polarizations, respectively.

Fig. 6 shows $S(\mathbf{Q}, \omega)_{\text{RIXS}}$ where regions with relative small error bars are selected, i.e., σ grazing-in, π grazing-out for LCO001, while σ grazing-out and π grazing-in for

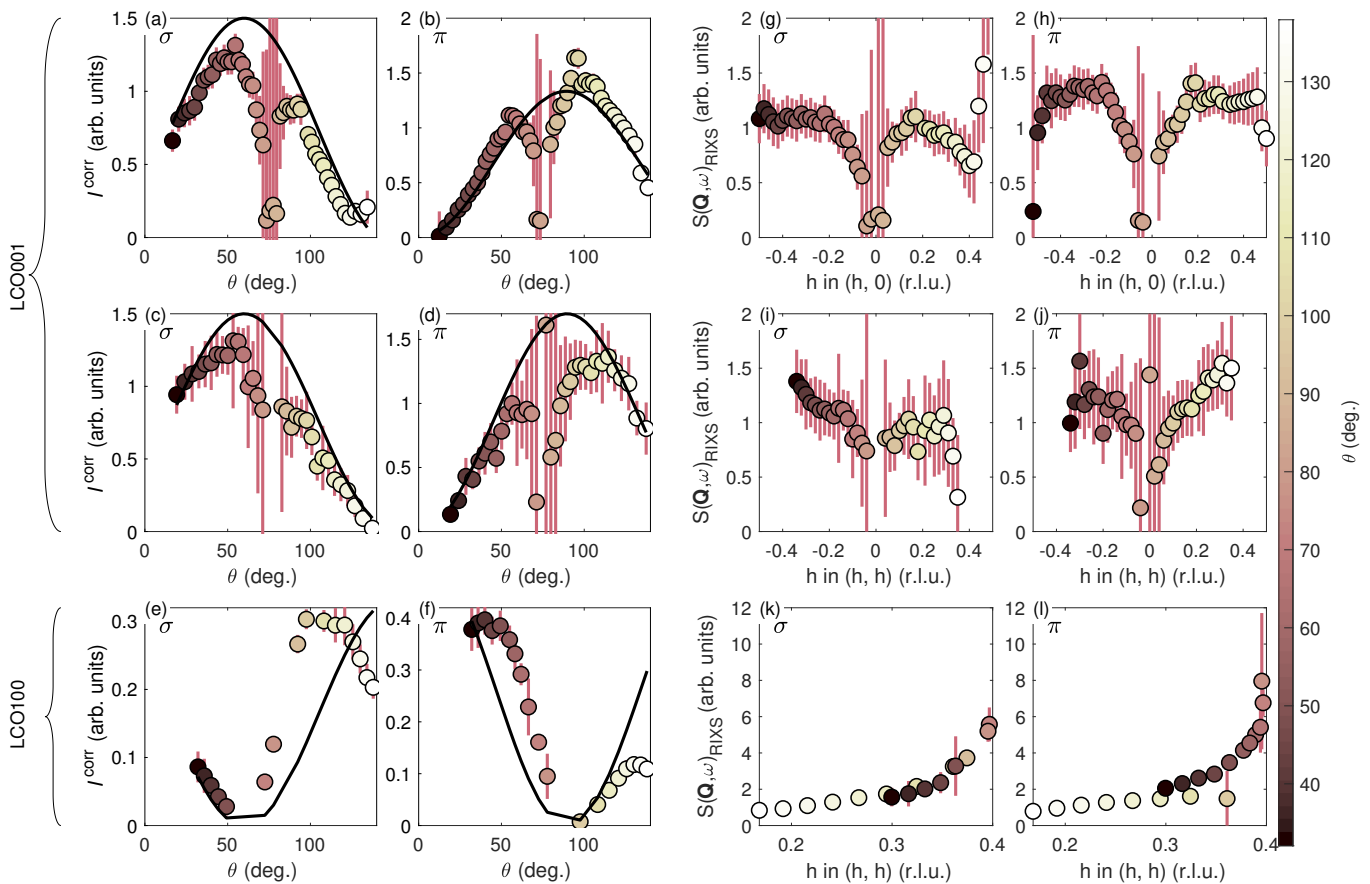


FIG. 5. Details of the deconvolution procedure for the magnon intensity. Panels (a-f) show the self-absorption corrected magnon intensity, I_{corr} (filled circles), compared to the single-ion spin-flip cross-section R_{spin} (black line). Panels (g-l) show the fully deconvoluted intensity, $S(\mathbf{Q}, \omega)_{\text{RIXS}}$ as a function of \mathbf{Q} . The value of θ is indicated by the colour.

LCO100. We also plot the magnon intensity measured with INS by Headings *et al.* [16] for the overlapped momentum space. Note that a single scaling constant is applied to the RIXS data in order to compare with INS data. In addition, we plot the spin-wave intensity calculated from the next-next nearest neighbour SWT model.

Along the $(h, 0)$ direction, both INS and RIXS show an approximately constant magnon intensity profile from 0.2 to 0.5 *r.l.u.*. Such behavior is a clear deviation from the linear spin-wave theory which increases monotonically approaching the zone boundary. The effect is explained in INS study due to the creation of a spinon pair [16]. INS measurements were only made up to 450 meV and it is interesting to note that RIXS measurements up to 1 eV yield similar results. This in turn demonstrates that the discrepancy at the zone boundary of $(1/2, 0)$ between the experimental results and the SWT is genuine. Along the (h, h) direction, LCO100 shows a sharp intensity increase towards the $\mathbf{Q}_{\text{AFM}} = (1/2, 1/2)$. We see vague indication of the trend in LCO001, however, the measurements do not reach large enough \mathbf{Q} . The measurements on LCO100 allows us to reach $(0.4, 0.4)$ which is crucial for the comparison with INS experimental data. The level of agreement is good among RIXS, INS and SWT model which

all show an increased intensity toward the $\mathbf{Q}_{\text{AFM}} = (1/2, 1/2)$. At low \mathbf{Q} , RIXS generally observes greater spectral weight than INS. The additional intensity may well result from the specular reflection influencing the magnon fits.

The intensity of the multimagnon excitations, which are well resolved in our data, could be extracted and corrected in the same way as the single magnons. However, in this instance the scattered polarisation is not well understood and the photon out polarisation analysis is necessary to separate components of the multimagnon continuum. The single-site calculations are also not adequate in this case as multimagnon creation is likely to be more complex [17, 39]. Cluster calculations are needed to provide a proper description of the multiple-sites spin-flip cross-section before the extraction of the dynamical spin susceptibility of the multimagnons.

V. CONCLUSIONS AND OUTLOOK

We have made high-resolution RIXS measurements of the orbital and collective magnetic excitation for La_2CuO_4 single crystals with the surface normals (001)

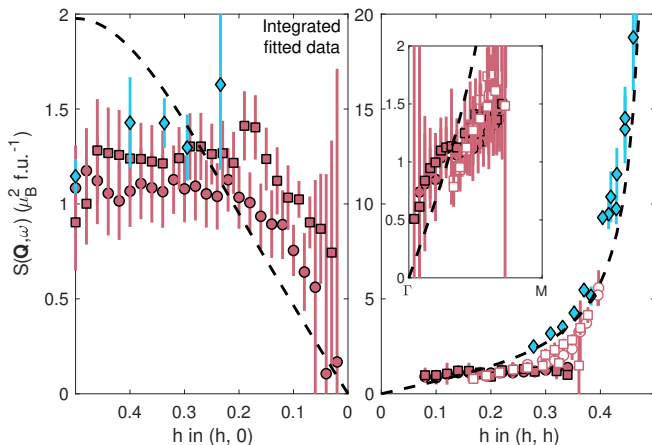


FIG. 6. Comparison of the spin-wave intensity for RIXS, INS and the theoretical values from SWT. INS data are shown as blue diamonds and the SWT as a black dashed line. RIXS data from the LCO100 and LCO100 orientation are indicated in pink and white marks, respectively, and σ and π polarisation are represented by circles and squares, respectively.

and (100). The spin-flip assisted dd orbital excitations are clearly resolved owing to the high energy resolution. Strong θ -dependence of the orbital excitations are well reproduced by the multiplet crystal field theory. The momentum-dependent collective magnetic excitations are measured along both $(h, 0)$ and (h, h) directions of the first Brillouin zone to the extent that is possible at the Cu L_3 -edge. The dispersion of the single magnons show a very good match to the spin-wave theory. Remarkably, the RIXS single magnon spectral profiles are reminiscent of those measured by INS. We determined the wavevector-dependent single-magnon response by correcting for the self-absorption and the local spin-flip RIXS matrix element. It is found that this response reflects the known dynamical spin susceptibility for La_2CuO_4 regardless of the incident photon polarization and the many-body effects involved in the RIXS process. Comparing to INS data, RIXS show excellent agreement along both primary directions. In particular, the consistent results between RIXS and INS show strong deviation from the spin-wave theory indicating the abnormal spin susceptibility approaching $(h, 0)$ zone boundary is a genuine behavior of the system.

Our results have several important implications. The established method of retrieving the pure spin susceptibility is readily applicable to doped cuprate superconductors. This is due to the existence of the fundamental matrix elements irrespective of the parent or the doped cuprate compounds. RIXS is able to make accurate reliable measurements of the spin susceptibility. Furthermore, the new method is also beneficial to spin susceptibility studies of many magnetic transition metal oxides. For instance, RIXS has revealed the magnetic excitations in 214 nickelates whose dispersions are consistent to that obtained with INS [40, 41]. As the local spin-flip cross-

section can be easily computed in these $3d^8$ systems, the study of the spin susceptibility will enable closer comparison with INS results. Finally, RIXS is unique in probing the higher-order, such as quadrupolar, magnetic excitations [42]. Applying the method to the study of the spin susceptibility of these higher-ranked magnetic orders is vital to systems like Kitaev quantum spin liquids.

ACKNOWLEDGMENTS

K.J.Z. and S.M.H. acknowledge J. van den Brink for fruitful discussions. The authors acknowledge funding and support from the Engineering and Physical Sciences Research Council (EPSRC) Centre for Doctoral Training in Condensed Matter Physics (CDT-CMP), Grant No. EP/L015544/1 as well as Grant No. EP/R011141/1. We acknowledge Diamond Light Source for providing the beamtime under the proposal SP18469 and the science commissioning time on the Beamline I21. We acknowledge Thomas Rice for the technical support throughout the beamtime. We would also like to thank the Materials Characterisation Laboratory team for help on the Laue instrument in the Materials Characterisation Laboratory at the ISIS Neutron and Muon Source.

Appendix A: Experimental details

1. Sample preparation

Samples of single-crystal LCO were grown via the travelling-solvent floating zone technique (TSFZ), annealed in an Argon atmosphere to remove excess oxygen, detwinned and cleaved *in-situ*. The crystals were previously used in the neutron scattering measurements described in reference [16].

2. Data processing

RIXS data are extracted by integrating along the non energy-dispersive direction at each \mathbf{Q} after subtracting the dark-image background. Spectra are normalised by the counting time. The zero-energy positions of RIXS spectra were determined by comparing to reference spectra recorded from the amorphous carbon tapes next to the sample for each \mathbf{Q} position. They were finely adjusted through the Gaussian fitting of each elastic peak. It is clear that this process is much easier close to the specular position ($\mathbf{Q} = 0$ in the LCO001 orientation) where the elastic peak becomes large. To reflect this, the error in the energy correction is established by the error in fitting a Gaussian peak multiplied by a Bose function $n(\omega)+1$ to model the excitations near $\omega = 0$. The shift in energy remains within 12 meV throughout the \mathbf{Q} -range, therefore we conclude that the procedure is consistent regardless of the intensity of the elastic peak.

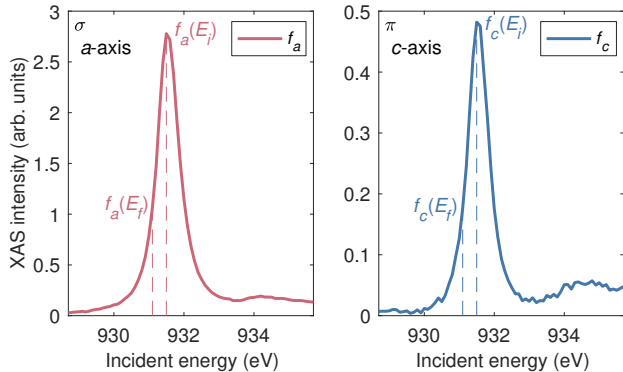


FIG. 7. The projected XAS spectra along the a - and c -axes in LCO samples with σ and π polarisations. $f_a(E_i)$, $f_c(E_i)$ have fixed intensity due to the fixed incident energy while $f_a(E_f)$, $f_c(E_f)$ of emitted X-rays are energy dependent.

3. Self-absorption correction

We follow recent practice [30, 43–46] to correct for the effects of self-absorption in our data using x-ray absorption spectra (XAS) measured in the same geometry as the RIXS measurements. We estimate a self-absorption factor, C_{SA} using the same procedure as outlined in reference [27], where the corrected intensity $I_{\sigma(\pi)}^{corr}$ is $I_{\sigma(\pi)}^{corr} = C_{SA} I_{\sigma(\pi)}^{meas}$ or,

$$I_{\sigma(\pi)}^{corr} = I_{\sigma(\pi)}^{meas} \frac{\mu_{i,\sigma(\pi)} \sin(\Omega - \theta) + \mu_{f,\sigma(\pi)} \sin \theta}{\sin(\Omega - \theta)}. \quad (A1)$$

Here μ_i and μ_f are the absorption coefficients extracted from XAS performed prior to the RIXS measurements. In our experiments the XAS is measured with the total electron yield. Components of the photon form factor, f_a and f_c , are extracted from the XAS intensity when the electric field of the incident x-rays is parallel to the crystalline a and c axes respectively which can be accessed with σ and π polarised x-rays respectively. Fig. 7 shows example XAS spectra measured along the a and c -axes. f_a and f_c are found from the intensity of the XAS spectra at E_i and E_f relative to the intensity at resonance. These values allow us to estimate the absorption coefficients for the incident and outgoing x-rays in the LCO001 geometry,

$$\begin{aligned} \mu_{i,\sigma} &= f_a(E_i), \\ \mu_{i,\pi} &= f_a(E_i) \sin^2 \theta + f_c(E_i) \cos^2 \theta, \\ \mu_{f,\sigma} &= f_a(E_f), \\ \mu_{f,\pi} &= f_a(E_f) \sin^2(\Omega - \theta) + f_c(E_f) \cos^2(\Omega - \theta). \end{aligned} \quad (A2)$$

For LCO100 the absorption coefficients can be approximated as,

$$\begin{aligned} \mu_{i,\sigma} &= f_a(E_i), \\ \mu_{i,\pi} &= f_c(E_i) \sin^2 \theta + f_a(E_i) \cos^2 \theta, \\ \mu_{f,\sigma} &= f_a(E_f), \\ \mu_{f,\pi} &= f_c(E_f) \sin^2(\Omega - \theta) + f_a(E_f) \cos^2(\Omega - \theta). \end{aligned} \quad (A3)$$

Taking these factors into account, Fig. 8 shows the energy, angle and polarisation dependence of the self-absorption factor, C_{SA} . A peak in self-absorption is seen close to the elastic position which is most pronounced at large θ . However, it is clear that there is significant variation in the extent of self-absorption depending on the experimental setup.

Fig. 9 shows the result of applying the self-absorption correction to the different excitations that were measured. Panels (a-f) show the dd excitations intensity before and after the self-absorption correction. As shown in Fig. 8, at the energy where the dd excitations occur, $\simeq 2$ eV, the self-absorption factor is relatively low, therefore the corrected intensity is not significantly changed. For dd excitations, we assume that the polarisation of the scattered photons is unchanged ($\sigma \rightarrow \sigma$ or $\pi \rightarrow \pi$). This is an approximation that does not account for the complexity of the dd excitations reported in reference [46] but as the total self-absorption at this energy is so small, this approximation works well enough for our purposes.

At low energy, the self-absorption is much greater and polarisation-dependence of the scattered light also becomes more significant. Fig. 9 (g-l) show the intensity of the single magnon excitations before and after the self-absorption correction. Here we assume the photon polarisation is flipped as a result of the excitation ($\sigma \rightarrow \pi$ or $\pi \rightarrow \sigma$). This assumption is justified by RIXS measurements performed with polarisation analysis such as that by Peng *et al.* [38] and Fumagalli *et al.* [46]. Following this assumption, the single magnon intensity is seen to be significantly altered by the self-absorption effects.

Appendix B: crystal field theory multiplet calculations

We computed the single-ion dd orbital and spin-flip excitations using crystal field theory implemented in the Quanta package [28, 29]. We define the ground and excited states and introduce interaction tensors between them. In both states the Cu^{2+} basis has D_{4h} symmetry with five orbitals, $d_{x^2-y^2}$, d_{z^2} , d_{xy} and $d_{xz/xy}$. The energies of these orbitals are obtained through fittings showing good consistency with previous RIXS measurements [33]. We summarise the values in Table I.

Three interaction tensors act on these bases. The first, U_{dd} describes the Coulomb repulsion between the $3d$ electrons. In Quanta, U_{dd} is expanded as a sum of spherical harmonics and is defined with three Slater integrals, F_{dd}^0 , F_{dd}^2 and F_{dd}^4 . Additional Coulomb interaction between

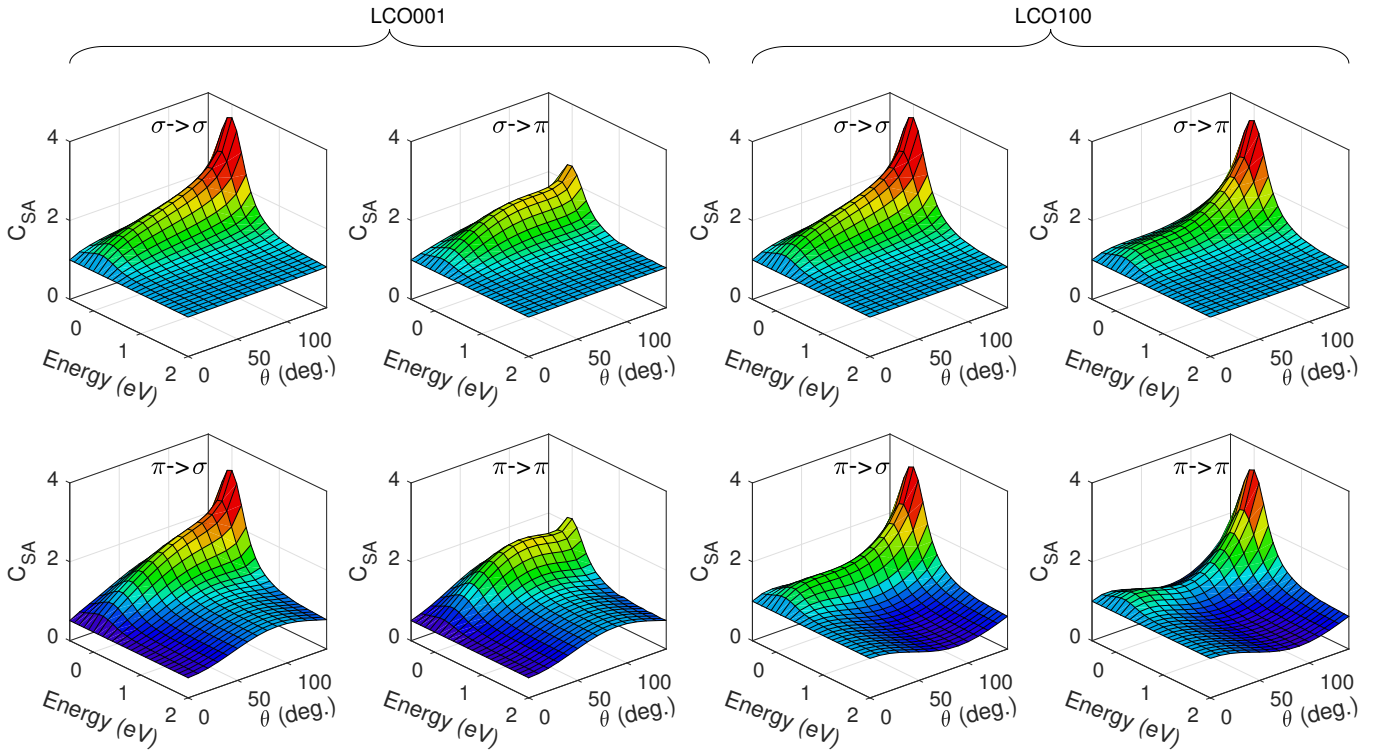


FIG. 8. The calculated self-absorption factor, C_{SA} for excitations measured in LCO as a function of excitation energy relative to Cu L_3 edge, incident angle θ and polarisation.

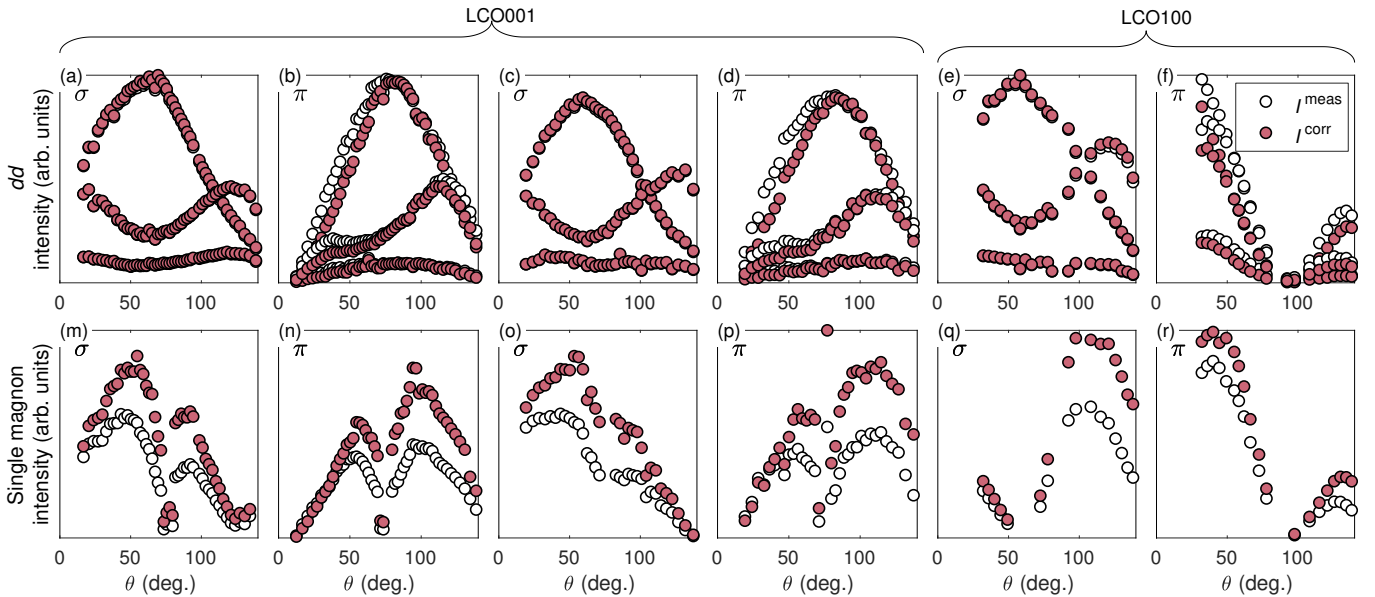


FIG. 9. RIXS intensity before and after applying the self-absorption correction. Measured data are shown in white and corrected data in red. The effect is shown for dd excitations in panels (a-f) and in single magnons in panels (g-l).

the $2p$ core hole and $3d$ electrons are defined by F_{pd}^0 and F_{pd}^2 . The second interaction tensor defines the exchange-Coulomb interaction between the $2p$ core hole and $3d$ electrons in the intermediate state and are given by Slater integrals G_{pd}^1 and G_{pd}^3 . The third interactions is spin-

orbit coupling which is defined for the ground state and the core-hole state, ξ_d and ξ_{2p} , respectively. To simulate the local spin-flip excitations, an inter-atomic exchange integral H_{exch} is introduced. The parameters used here are given in Table II.

$d_{x^2-y^2}$ (eV)	d_{z^2} (eV)	d_{xy} (eV)	d_{xz} (eV)	d_{yz} (eV)
0	1.5	1.8	2.1	2.1

TABLE I. Values of the orbital energies in LCO relative to the $d_{x^2-y^2}$ orbital. Parameters are obtained from RIXS measurements in reference [33] and used in the single-site multiplet crystal field theory calculations of the local interactions.

	F_{dd}^0	F_{dd}^2	F_{dd}^4	F_{pd}^0	F_{pd}^2	G_{pd}^1	G_{pd}^3	ζ_d	ζ_{2p}
$2p^6 3d^9$	0	12.854	7.980					0.102	
$2p^5 3d^{10}$	0	13.611	8.457	0	8.177	6.169	3.510	0.124	13.498

TABLE II. Parameters used in the single-site multiplet crystal field theory calculations of the local interactions in LCO. Parameters are from reference [47].

- [1] G. R. Stewart, *Heavy-fermion systems*, Rev. Mod. Phys. **56**, 755 (1984).
- [2] J. G. Bednorz and K. A. Müller, *Possible high T_c superconductivity in the Ba-La-Cu-O system*, Zeitschrift für Physik B Condensed Matter **64**, 189 (1986).
- [3] Y. Maeno, H. Hashimoto, K. Yoshida, S. Nishizaki, T. Fujita, J. G. Bednorz, and F. Lichtenberg, *Superconductivity in a layered perovskite without copper*, Nature **372**, 532 (1994).
- [4] Y. Kamihara, H. Hiramatsu, M. Hirano, R. Kawamura, H. Yanagi, T. Kamiya, and H. Hosono, *Iron-based layered superconductor: LaOFeP*, J. Am. Chem. Soc. **128**, 10012 (2006).
- [5] D. J. Scalapino, *A common thread: The pairing interaction for unconventional superconductors*, Rev. Mod. Phys. **84**, 1383 (2012).
- [6] K. B. Lyons, P. A. Fleury, L. F. Schneemeyer, and J. V. Waszczak, *Spin fluctuations and superconductivity in $Ba_2 YCu_3 O_{6+\delta}$* , Phys. Rev. Lett. **60**, 732 (1988).
- [7] S. M. Hayden, G. Aeppli, H. A. Mook, T. G. Perring, T. E. Mason, S.-W. Cheong, and Z. Fisk, *Comparison of the high-frequency magnetic fluctuations in insulating and superconducting $La_{2-x}Sr_xCuO_4$* Phys. Rev. Lett. **76**, 1344 (1996).
- [8] P. Dai, H. A. Mook, R. D. Hunt, and F. Doğan, *Evolution of the resonance and incommensurate spin fluctuations in superconducting $YBa_2Cu_3O_{6+x}$* , Phys. Rev. B **63**, 054525 (2001).
- [9] C. Stock, W. J. L. Buyers, R. A. Cowley, P. S. Clegg, R. Coldea, C. D. Frost, R. Liang, D. Peets, D. Bonn, W. N. Hardy, and R. J. Birgeneau, *From incommensurate to dispersive spin-fluctuations: The high-energy inelastic spectrum in superconducting $YBa_2Cu_3O_{6.5}$* , Phys. Rev. B **71**, 024522 (2005).
- [10] O. J. Lipscombe, S. M. Hayden, B. Vignolle, D. F. McMorrow, and T. G. Perring, *Persistence of high-frequency spin fluctuations in overdoped superconducting $La_{2-x}Sr_xCuO_4$ ($x=0.22$)*, Phys. Rev. Lett. **99**, 067002 (2007).
- [11] N. S. Headings, S. M. Hayden, J. Kulda, N. H. Babu, and D. A. Cardwell, *Spin anisotropy of the magnetic excitations in the normal and superconducting states of optimally doped $YBa_2Cu_3O_{6.9}$ studied by polarized neutron spectroscopy*, Phys. Rev. B **84**, 104513 (2011).
- [12] M. Dean, *Insights into the high temperature superconducting cuprates from resonant inelastic X-ray scattering*, J. Magn. Magn. Mater. **376**, 3 (2015).
- [13] D. Scalapino, *The case for $d_{x^2-y^2}$ pairing in the cuprate superconductors*, Physics Reports **250**, 329 (1995).
- [14] G. L. Squires, *Introduction to the theory of neutron scattering* (Cambridge University Press, 1978).
- [15] R. Coldea, S. M. Hayden, G. Aeppli, T. G. Perring, C. D. Frost, T. E. Mason, S.-W. Cheong, and Z. Fisk, *Spin waves and electronic interactions in La_2CuO_4* , Phys. Rev. Lett. **86**, 5377 (2001).
- [16] N. S. Headings, S. M. Hayden, R. Coldea, and T. G. Perring, *Anomalous high-energy spin excitations in the high- T_c superconductor-parent antiferromagnet La_2CuO_4* , Phys. Rev. Lett. **105**, 247001 (2010).
- [17] L. J. P. Ament, G. Ghiringhelli, M. M. Sala, L. Braicovich, and J. van den Brink, *Theoretical demonstration of how the dispersion of magnetic excitations in cuprate compounds can be determined using resonant inelastic X-ray scattering*, Phys. Rev. Lett. **103**, 117003 (2009).
- [18] L. J. Ament, M. Van Veenendaal, T. P. Devereaux, J. P. Hill, and J. Van Den Brink, *Resonant inelastic x-ray scattering studies of elementary excitations*, Rev. Mod. Phys. **83**, 705 (2011).
- [19] L. Braicovich, J. van den Brink, V. Bisogni, M. M. Sala, L. J. P. Ament, N. B. Brookes, G. M. De Luca, M. Saluzzo, T. Schmitt, V. N. Strocov, and G. Ghiringhelli, *Magnetic excitations and phase separation in the underdoped $La_{2-x}Sr_xCuO_4$ superconductor measured by resonant inelastic X-ray scattering*, Phys. Rev. Lett. **104**, 077002 (2010).

- [20] M. P. M. Dean, R. S. Springell, C. Monney, K. J. Zhou, J. Pereiro, I. Božović, B. Dalla Piazza, H. M. Rønnow, E. Morenzoni, J. van den Brink, T. Schmitt, and J. P. Hill, *Spin excitations in a single La_2CuO_4 layer*, Nat. Mater. **11**, 850 (2012).
- [21] M. P. M. Dean, G. Dellea, R. S. Springell, F. Yakhour-Harris, K. Kummer, N. B. Brookes, X. Liu, Y.-J. Sun, J. Strle, T. Schmitt, L. Braicovich, G. Ghiringhelli, I. Božović, and J. P. Hill, *Persistence of magnetic excitations in $\text{La}_{2-x}\text{Sr}_x\text{CuO}_4$ from the undoped insulator to the heavily overdoped non-superconducting metal*, Nat. Mater. **12**, 1019 (2013).
- [22] M. P. M. Dean, A. J. A. James, R. S. Springell, X. Liu, C. Monney, K. J. Zhou, R. M. Konik, J. S. Wen, Z. J. Xu, G. D. Gu, V. N. Strocov, T. Schmitt, and J. P. Hill, *High-energy magnetic excitations in the cuprate superconductor $\text{Bi}_2\text{Sr}_2\text{CaCu}_2\text{O}_{8+\delta}$: Towards a unified description of its electronic and magnetic degrees of freedom*, Phys. Rev. Lett. **110**, 147001 (2013).
- [23] M. Guarise, B. D. Piazza, H. Berger, E. Giannini, T. Schmitt, H. M. Rønnow, G. A. Sawatzky, J. van den Brink, D. Altenfeld, I. Eremin, and M. Grioni, *Anisotropic softening of magnetic excitations along the nodal direction in superconducting cuprates*, Nat. Commun. **5**, 5760 (2014).
- [24] S. Wakimoto, K. Ishii, H. Kimura, M. Fujita, G. Dellea, K. Kummer, L. Braicovich, G. Ghiringhelli, L. M. Debeer-Schmitt, and G. E. Granroth, *High-energy magnetic excitations in overdoped $\text{La}_{2-x}\text{Sr}_x\text{CuO}_4$ studied by neutron and resonant inelastic x-ray scattering*, Phys. Rev. B **91**, 184513 (2015).
- [25] D. Meyers, H. Miao, A. C. Walters, V. Bisogni, R. S. Springell, M. d'Astuto, M. Dantz, J. Pellicciari, H. Y. Huang, J. Okamoto, D. J. Huang, J. P. Hill, X. He, I. Božović, T. Schmitt, and M. P. M. Dean, *Doping dependence of the magnetic excitations in $\text{La}_{2-x}\text{Sr}_x\text{CuO}_4$* , Phys. Rev. B **95**, 075139 (2017).
- [26] M. Le Tacon, G. Ghiringhelli, J. Chaloupka, M. M. Sala, V. Hinkov, M. Haverkort, M. Minola, M. Bakr, K. Zhou, and S. Blanco-Canosa *et al.*, *Intense paramagnon excitations in a large family of high-temperature superconductors*, Nat. Phys. **7**, 725 (2011).
- [27] H. Robarts, M. Barthélemy, K. Kummer, M. García-Fernández, J. Li, A. Nag, A. Walters, K. Zhou, and S. Hayden, *Anisotropic damping and wave vector dependent susceptibility of the spin fluctuations in $\text{La}_{2-x}\text{Sr}_x\text{CuO}_4$ studied by resonant inelastic x-ray scattering*, Phys. Rev. B **100**, 214510 (2019).
- [28] M. Haverkort, M. Zwierzycki, and O. Andersen, *Multiplet ligand-field theory using Wannier orbitals*, Phys. Rev. B **85**, 165113 (2012).
- [29] M. W. Haverkort, *Quanta for core level spectroscopy - excitons, resonances and band excitations in time and frequency domain*, J. Phys.: Conf. Ser. **712**, 012001 (2016).
- [30] M. Minola, G. Dellea, H. Gretarsson, Y. Y. Peng, Y. Lu, J. Porras, T. Loew, F. Yakhou, N. B. Brookes, Y. B. Huang, J. Pellicciari, T. Schmitt, G. Ghiringhelli, B. Keimer, L. Braicovich, and M. Le Tacon, *Collective nature of spin excitations in superconducting cuprates probed by resonant inelastic X-ray scattering*, Phys. Rev. Lett. **114**, 217003 (2015).
- [31] M. Kang, J. Pellicciari, Y. Krockenberger, J. Li, D. McNally, E. Paris, R. Liang, W. N. Hardy, D. A. Bonn, H. Yamamoto, *et al.*, *Resolving the nature of electronic excitations in resonant inelastic x-ray scattering*, Phys. Rev. B **99**, 045105 (2019).
- [32] G. Ghiringhelli, N. B. Brookes, E. Annese, H. Berger, C. Dallera, M. Grioni, L. Perfetti, A. Tagliaferri, and L. Braicovich, *Low energy electronic excitations in the layered cuprates studied by copper L_3 resonant inelastic X-Ray scattering*, Phys. Rev. Lett. **92**, 117406 (2004).
- [33] M. M. Sala, V. Bisogni, C. Aruta, G. Balestrino, H. Berger, N. B. Brookes, G. M. de Luca, D. Di Castro, M. Grioni, and M. Guarise *et al.*, *Energy and symmetry of dd excitations in undoped layered cuprates measured by Cu L_3 resonant inelastic x-ray scattering*, New J. Phys. **13**, 043026 (2011).
- [34] T. Devereaux, A. Shvaika, K. Wu, K. Wohlfeld, C. Jia, Y. Wang, B. Moritz, L. Chaix, W.-S. Lee, and Z.-X. Shen *et al.*, *Directly characterizing the relative strength and momentum dependence of electron-phonon coupling using resonant inelastic X-Ray scattering*, Phys. Rev. X **6**, 041019 (2016).
- [35] V. Bisogni, M. Moretti Sala, A. Bendounan, N. B. Brookes, G. Ghiringhelli, and L. Braicovich, *Bimagnon studies in cuprates with resonant inelastic x-ray scattering at the O K edge. II. Doping effect in $\text{La}_{2-x}\text{Sr}_x\text{CuO}_4$* , Phys. Rev. B **85**, 214528 (2012).
- [36] L. Chaix, E. Huang, S. Gerber, X. Lu, C. Jia, Y. Huang, D. E. McNally, Y. Wang, F. H. Vernay, and A. Keren *et al.*, *Resonant inelastic x-ray scattering studies of magnons and bimagnons in the lightly doped cuprate $\text{La}_{2-x}\text{Sr}_x\text{CuO}_4$* , Phys. Rev. B **97**, 155144 (2018).
- [37] C. Monney, T. Schmitt, C. E. Matt, J. Mesot, V. N. Strocov, O. J. Lipscombe, S. M. Hayden, and J. Chang, *Resonant inelastic x-ray scattering study of the spin and charge excitations in the overdoped superconductor $\text{La}_{1.77}\text{Sr}_{0.23}\text{CuO}_4$* , Phys. Rev. B **93**, 075103 (2016).
- [38] Y. Y. Peng, E. W. Huang, R. Fumagalli, M. Minola, Y. Wang, X. Sun, Y. Ding, K. Kummer, X. J. Zhou, and N. B. Brookes *et al.*, *Dispersion, damping, and intensity of spin excitations in the monolayer $(\text{Bi,Pb})_2(\text{Sr,L a})_2\text{CuO}_{6+\delta}$ cuprate superconductor family*, Phys. Rev. B **98**, 144507 (2018).
- [39] L. J. Ament and J. van den Brink, *Strong three-magnon Scattering in cuprates by resonant X-rays*, arXiv:1002.3773 (2010).
- [40] G. Fabbris, D. Meyers, L. Xu, V. Katukuri, L. Hozoi, X. Liu, Z.-Y. Chen, J. Okamoto, T. Schmitt, and A. Uldry *et al.*, *Doping dependence of collective spin and orbital excitations in the spin-1 quantum antiferromagnet $\text{La}_{2-x}\text{Ni}_x\text{CuO}_4$ observed by X rays*, Phys. Rev. Lett. **118**, 156402 (2017).
- [41] K. Nakajima, K. Yamada, S. Hosoya, T. Omata, and Y. Endoh, *Spin-wave excitations in two dimensional antiferromagnet of stoichiometric La_2NiO_4* , J. Phys. Soc **62**, 4438 (1993).
- [42] A. Nag, H. Robarts, F. Wenzel, J. Li, H. Elnaggar, R.-P. Wang, A. Walters, M. Garcia-Fernandez, F. de Groot, and M. Haverkort *et al.*, *Many-body physics of single and double spin-flip excitations in NiO* , Phys. Rev. Lett. **124**, 067202 (2020).
- [43] R. Comin, R. Sutarto, E. H. da Silva Neto, L. Chauviere, R. Liang, W. N. Hardy, D. A. Bonn, F. He, G. A. Sawatzky, and A. Damascelli, *Broken translational and rotational symmetry via charge stripe order in underdoped $\text{YBa}_2\text{Cu}_3\text{O}_{6+y}$* , Science **347**, 1335 (2015).
- [44] R. Comin, R. Sutarto, F. He, E. H. da Silva Neto, L.

- Chauviere, A. Fraño, R. Liang, W. N. Hardy, D. A. Bonn, Y. Yoshida, H. Eisaki, A. J. Achkar, D. G. Hawthorn, B. Keimer, G. A. Sawatzky, and A. Damascelli, *Symmetry of charge order in cuprates*, Nature Materials **14**, 796 (2015).
- [45] A. J. Achkar, F. He, R. Sutarto, C. McMahan, M. Zwiebler, M. Hücker, G. D. Gu, R. Liang, D. A. Bonn, W. N. Hardy, J. Geck, and D. G. Hawthorn, *Orbital symmetry of charge-density-wave order in $La_{1.875}Ba_{0.125}CuO_4$ and $YBa_2Cu_3O_{6.67}$* , Nat. Mater. **15**, 616 (2016).
- [46] R. Fumagalli, L. Braicovich, M. Minola, Y. Y. Peng, K. Kummer, D. Betto, M. Rossi, E. Lefrançois, C. Morawe, M. Salluzzo, H. Suzuki, F. Yakhou, M. Le Tacon, B. Keimer, N. B. Brookes, M. M. Sala, and G. Ghiringhelli, *Polarization-resolved Cu L_3 -edge resonant inelastic x-ray scattering of orbital and spin excitations in $NdBa_2Cu_3O_{7-\delta}$* , Phys. Rev. B **99**, 134517 (2019).
- [47] M. Haverkort, *Spin and orbital degrees of freedom in transition metal oxides and oxide thin films studied by soft x-ray absorption spectroscopy*, Ph.D. thesis, Universität zu Köln (2005).